Available online at www.sciencedirect.com
ScienceDirect
Trans. Nonferrous Met. Soc. China 33(2023) 1098−1113
Transactions of Nonferrous Metals Society of China
www.tnmsc.cn

Influence of $\alpha+\beta$ solution treatments on Ti65 ultrathin sheets: Silicide precipitation, mechanical behaviour and novel $\{10\bar{1}1\}$ twinning system

Ding ZHAO[1], Jiang-kun FAN[1,2,3], Zhi-xin ZHANG[1,4], Jing WANG[1], Qing-jiang WANG[5], Zhi-yong CHEN[5], Bin TANG[1,2], Hong-chao KOU[1,2], Jin-shan LI[1,2]

1. State Key Laboratory of Solidification Processing, Northwestern Polytechnical University, Xi'an 710072, China;
2. Innovation Center, NPU·Chongqing, Chongqing 401135, China;
3. National & Local Joint Engineering Research Center for Precision Thermoforming Technology of Advanced Metal Materials, Northwestern Polytechnical University, Xi'an 710072, China;
4. Baoti Group Ltd., Baoji 721014, China;
5. Institute of Metal Research, Chinese Academy of Sciences, Shenyang 110016, China

Received 22 November 2021; accepted 29 March 2022

Abstract: To cope with the urgent demands of the aerospace industry for lightweight and excellent high-temperature performance titanium alloy components, the microstructure evolution, silicide precipitation and mechanical behaviour of a novel high-temperature Ti65 titanium alloy ultrathin sheet with different heat treatments were systematically investigated. Submicron $(Ti,Zr)_6Si_3$ silicides are observed after solution treatments followed by air cooling, leading to a decline and significant fluctuations in tensile properties. For furnace cooling samples, $(Ti,Zr)_5Si_3$ silicide crossing grain boundaries and $(Ti,Zr)_6Si_3$ silicide near grain boundaries are observed after solution treatment at 950 ℃. When the solution temperature increases to 1010 ℃, the third silicide $(Ti,Zr)_3Si$ appears near dislocations. The combined effect of the strong size effect of the alloy ultrathin sheet and silicide precipitation results in great performance fluctuation, sharp drop of ductility and even brittle fracture. In addition, silicide precipitation differs little with various holding time during low-temperature solution treatment. Moreover, novel $\{10\bar{1}1\}$ twins appear after the rolling process at 990 ℃ and are only inside coarse basal texture α grains, with an axis−angle pair of $65°\langle 84\bar{4}3\rangle$.
Key words: titanium alloy; ultrathin sheet; silicide; mechanical property; size effect; twinning

1 Introduction

With high strength, low density and exceptional high-temperature performance, titanium materials have been widely used in the aerospace sector [1,2]. In recent years, there are further demands for lightweight and high-strength aerospace components. To cope with urgent demands, titanium ultrathin sheets have been applied [3], such as TC4 alloys with honeycomb sandwich structures. In contrast to the mechanical behaviour of bars and sheets [4,5], pronounced differences in the mechanical properties and processing capabilities of ultrathin sheets are observed owing to the thickness decrease [6,7]. The novel near-α titanium Ti65 alloy (Ti−Al−Sn−Zr−Mo−Si−Nb−Ta−W−C) shows a long-term service temperature up to 600−650 ℃ [8], a high performance that was unattainable before. The high service temperature makes it possible for Ti65 ultrathin sheets to be used as honeycomb sandwiches in turbofan engines. However, silicide precipitation occurred after heat treatments, which can significantly influence mechanical behaviour. In addition, a novel twin was observed in as-rolled

Corresponding author: Jiang-kun FAN, Tel: +86-18702988608, E-mail: jkfan@nwpu.edu.cn
DOI: 10.1016/S1003-6326(23)66168-0

Ti65 ultrathin sheet. Thus, to clarify the microstructure evolution mechanism and further improve the mechanical properties of Ti65 ultrathin sheets, systematic investigations on silicide precipitation after heat treatments and the corresponding mechanical behaviour are essential.

Generally, silicide precipitation in high-temperature titanium alloys occurs after the ageing process. Three common types of silicides are listed below: (1) Ti_5Si_3 silicide (S1-type, hexagonal) is more likely to precipitate during low-temperature ageing; (2) Ti_6Si_3 silicide (S2-type, hexagonal) precipitates during high-temperature ageing; (3) Ti_3Si silicide (S3-type, tetragonal) can only be observed during long-term ageing at high temperature (below 1170 ℃) due to the limit of its low formation rate [9,10]. The influence of silicide precipitation can be split into two parts. First, silicide precipitation results in a stronger precipitation strengthening effect but with a weaker solid solution strengthening effect due to depleted solution elements in the matrix. ZHANG et al [11] attributed the strengthening of aged Ti65 sheets to silicide precipitation. In contrast, the BTi−6431S alloy showed degradation of mechanical properties after silicide precipitation, as reported by ZHANG et al [12]. In addition, silicide promotes the initiation of voids and fatigue crack growth [13]. In the case of ultrathin sheets, the rapid cooling rate and the size effect arising from the extreme specimen dimension can significantly affect the precipitation of silicides.

Twenty-six twinning systems in α-Ti have been theoretically identified, while only $\{10\bar{1}2\}$, $\{11\bar{2}1\}$, $\{11\bar{2}3\}$, $\{10\bar{1}1\}$, $\{11\bar{2}2\}$ and $\{11\bar{2}4\}$ twinning systems are widely reported. In general, high temperature inhibits the activation of twinning systems. However, the $\{10\bar{1}1\}$ twinning system can only be activated at high temperature. Because the critical activation stress decreases with increasing temperature [14], the difficulty of $\{10\bar{1}1\}$ twinning activation is inversely proportional to temperature [15]. PATON and BACKOFEN [16] proposed that a $\{10\bar{1}1\}$ twinning system can be activated in the temperature interval of 400−800 ℃. A similar conclusion was drawn by ZENG et al [17], in which $\{10\bar{1}1\}$ twinning was observed at temperatures ranging from 400 to 700 ℃. However, no twinning formation at higher temperatures has been reported, owing to the dominant role of the slip system at elevated temperatures.

As a novel high-temperature titanium alloy with a temperature resistance of 650 °C, the silicide precipitation during heat treatments and the new twinning characteristics found during the rolling deformation of Ti65 alloy ultrathin sheets need to be further revealed, especially in the case of ultrathin sheets where typical size effects may exist. Hence, in order to investigate the mechanism of the influence of silicides on the mechanical properties under size effect, the microstructure evolution and mechanical behaviour of the Ti65 alloy ultrathin sheet after the solution heat treatments are systematically studied in this work. The precipitation behaviour of diverse silicides is analysed by quantitative statistics using transmission electron microscopy (TEM) and energy dispersive spectrometry (EDS). The size effect inherent in ultrathin sheet materials is also discussed in depth. In addition, the novel twinning system is determined based on crystallographic orientation acquisition and analysis by electron back scattering diffraction (EBSD). The main results and conclusions are expected to provide help and reference for microstructure evolution and mechanical behaviour improvement of near-α titanium alloy ultrathin sheets.

2 Experimental

A Ti65 ultrathin sheet with a thickness of 0.5 mm was obtained by pack ply rolling along the rolling direction at 990 ℃. The chemical composition is Ti−5.4Al−3.82Sn−3.18Zr−0.51Mo−0.37Si−0.27Nb−0.92Ta−0.71W−0.06C (wt.%), and the β phase transus temperature obtained via optical microscopy was 1035 ℃. Samples were heat treated by vacuum sealing with a vacuum degree of 6×10^{-4} Pa, and the specific heat treatments are listed in Table 1. For simplicity, samples are coded as an abbreviation of the solution temperature-holding time-cooling medium, such as 950 ℃-2 h-AC (AC represents air cooling and FC stands for furnace cooling). Tensile specimens with a size of 30 mm × 50 mm (parallel to RD) are shown in Fig. 1, in which RD, TD and ND represent the rolling, transverse and normal directions of the as-rolled sheet. Tensile tests were carried out on an ETM105D universal testing

machine along RD at ambient temperature, with a strain rate of 5×10^{-4} s^{-1}. The strain was measured by an electronic extensometer. Repeated tests were carried out in each case to ensure the accuracy of the experimental data.

Table 1 Heat treatments applied to Ti65 alloy ultrathin sheets

Solution temperature/℃	Holding time/h	Cooling
950	0.25, 2, 4, 8, 24	Air cooling (AC)
950	0.5, 2, 4	Furnace cooling (FC)
950, 970, 990, 1010	2	Furnace cooling (FC)

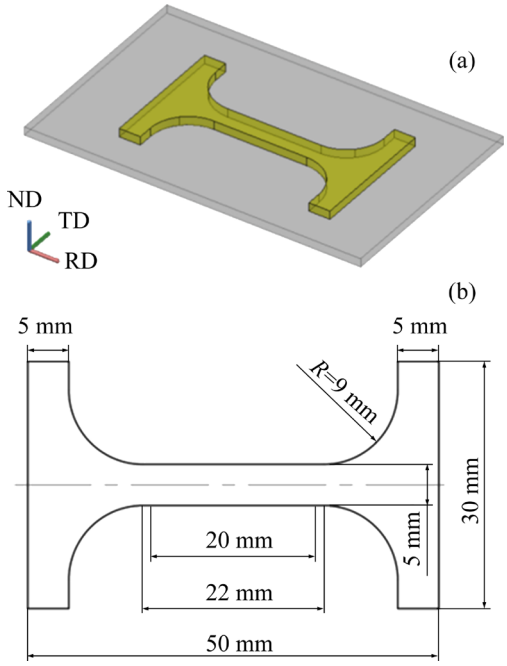

Fig. 1 Schematic of tensile test directions (RD, TD and ND represent rolling, transverse and normal directions of as-rolled sheet, respectively) (a), and geometry and dimension of tensile test specimens (b)

The metallographic examination samples were prepared through mechanical grinding, polishing and subsequent etching by an electrolyte of V(HF):V(HNO_3):V(H_2O)=1:1:50. The microstructure and fracture morphology observations were performed by using a ZEISS Gemini 500 field emission scanning electron microscope (SEM). Point scanning and map scanning results were acquired by the same microscope to determine the chemical composition of the precipitation phase and element distribution. EBSD specimens were prepared by electropolishing in a solution of 5 mL perchloric acid, 35 mL butyl alcohol and 60 mL methanol at 35 V and 5 ℃ for 25−30 s. EBSD tests were performed by an FEI Helios G4 CX focused ion beam SEM equipped with an EBSD scanner, and a step size of 0.3 μm was applied in each case to eliminate errors during grain detection. The EBSD data analyses were carried out by HKL Channel 5 software; hence, inverse pole figure (IPF) maps were obtained. Grain boundaries with misorientation higher than 15° are denoted as high angle grain boundaries (HAGBs) and by thick black lines, while low angle grain boundaries (LAGBs) with misorientation lower than 15° are not shown. TEM specimens for silicide calibration were prepared by grinding ultrathin sheets to 50 μm in thickness, punching out wafers of 3 mm in diameter, and finally thinning of finished samples by a twinjet machine using an electrolyte of 20% perchloric acid in methanol at 5 ℃ and 35 V. The TEM specimens for twinning analyses were obtained by focused ion beam (FIB) on the FEI Helios G4 CX FIB SEM. TEM tests were performed by a Talos F200X field high-resolution TEM. Bright field (BF) images and dark field (DF) images were captured to analyse silicide precipitation and twinning system activation.

3 Results

3.1 Solution treatments followed by air cooling

3.1.1 Microstructure evolution

Micrographs of Ti65 alloy ultrathin sheet samples after solution treatments followed by air cooling are shown in Fig. 2. The typical equiaxed structure in the as-rolled sample consists of equiaxed primary α (α_p), lamellar secondary α (α_s) and a few β phases. Almost no elongated α_p is observed in the as-rolled sample as a result of spheroidization and dynamic recrystallization during hot rolling. Compared to the as-rolled sample, the average α grain size does not change much after 0.25 h solution treatment, whereas numerous ellipsoidal precipitates appear near grain boundaries, as shown in the illustration of Fig. 2(d). Based on the alloy composition and previous studies, the precipitates are preliminarily determined as silicides. With increasing holding time, no significant changes in the size or volume fraction of silicides can be observed. In addition, the lamellar thickness of α_s is significantly reduced,

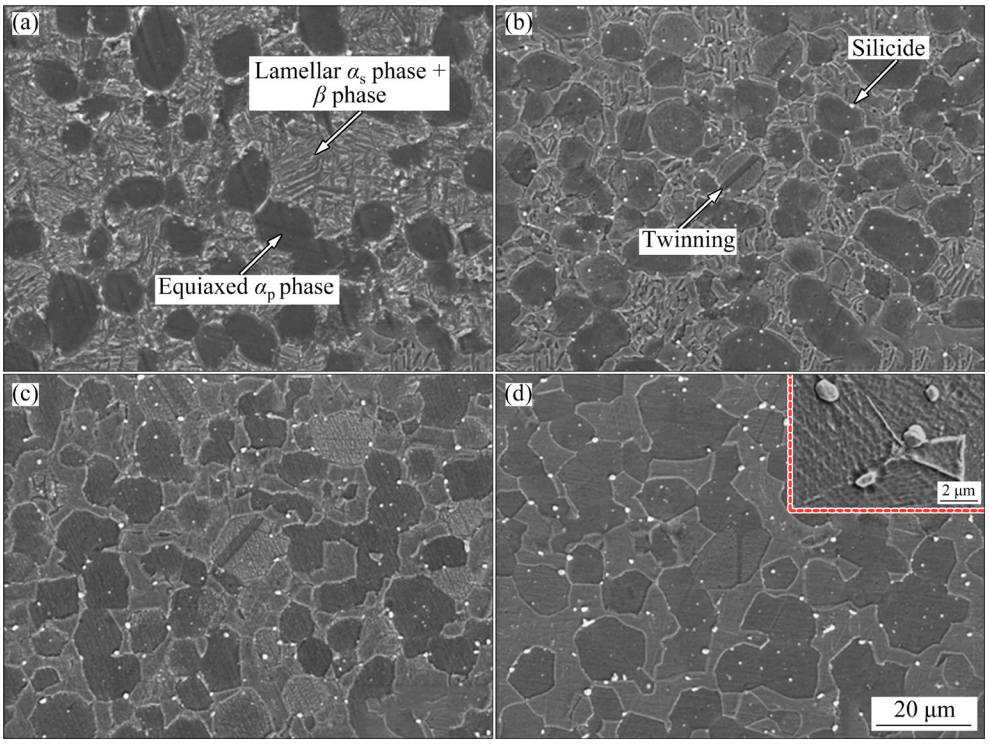

Fig. 2 Micrographs of Ti65 alloy ultrathin sheet samples after solution treatments followed by air cooling: (a) As-rolled; (b) 950 ℃-0.25 h-AC; (c) 950 ℃-4 h-AC; (d) 950 ℃-8 h-AC

and the grain boundaries of α_p become flatter. Finally, a small amount of twinning is observed, but only inside equiaxed α_p phases.

3.1.2 $(Ti,Zr)_6Si_3$ silicide precipitation

The type of silicide was determined by map scanning and point scanning. The enrichment of silicon and zirconium and the depletion of titanium in the vicinity of the precipitates are displayed in Fig. 3(a), which are typical of silicide precipitation. The distribution of tin here is homogeneous, which is contrary to tin enrichment observed in Ti65 alloy bars after silicide precipitation [18]. In addition, a weak niobium enrichment takes place.

The selected silicides of 950 ℃-0.25 h-AC (Fig. 3(b)) and 950 ℃-2 h-AC (Fig. 3(c)) samples during spot scanning are marked. The corresponding elemental composition results are listed in Table 2, and elemental composition data unrelated to the following analyses are omitted. The atomic ratio of (Ti,Zr)/Si in selected silicides ranges from 2.10 to 3.00. However, it is difficult for Ti_3Si silicide to precipitate after solution treatment at a relatively low temperature with a short holding time. In addition, the atomic ratio of Ti/Zr in selected silicides ranges from 1.51 to 2.25, which is consistent with the conclusion drawn by SALPADORU and FLOWER [19] that the atomic ratio of Ti/Zr in $(Ti,Zr)_6Si_3$ silicide is 0.68−2.26. Consequently, the possibility of Ti_3Si silicide precipitation is ruled out.

Figure 3(d) depicts the TEM characterization of silicides. Submicron silicides are distributed near grain boundaries. The selected-area-electron-diffraction (SAED) pattern acquired at the interface between the matrix and silicide indicates that the following orientational correlation is identified: $[1\bar{2}10]_{\alpha\text{-Ti}} // [0002]_{\text{Silicide}}$ and $(10\bar{1}1)_{\alpha\text{-Ti}} // (\bar{3}120)_{\text{Silicide}}$. The measured lattice parameter (a=0.702 nm, and c=0.368 nm) is consistent with the conclusion drawn by RAMACHANDRA and SINGH [20]. Furthermore, the atomic ratio of Ti/Zr/Si in the silicide marked in Fig. 3(d) is approximately 1:1:1. Hence, the silicide precipitates after solution treatments followed by air cooling are determined to be $(Ti,Zr)_6Si_3$.

The tensile test results of the air-cooled samples are listed in Table 3. As mentioned, the as-rolled and 950 ℃-0.25 h-AC samples manifest similar α grain sizes. However, the tensile properties show distinct differences owing to silicide precipitation. The ultimate tensile strength (UTS), tensile yield stress (TYS) and elongation

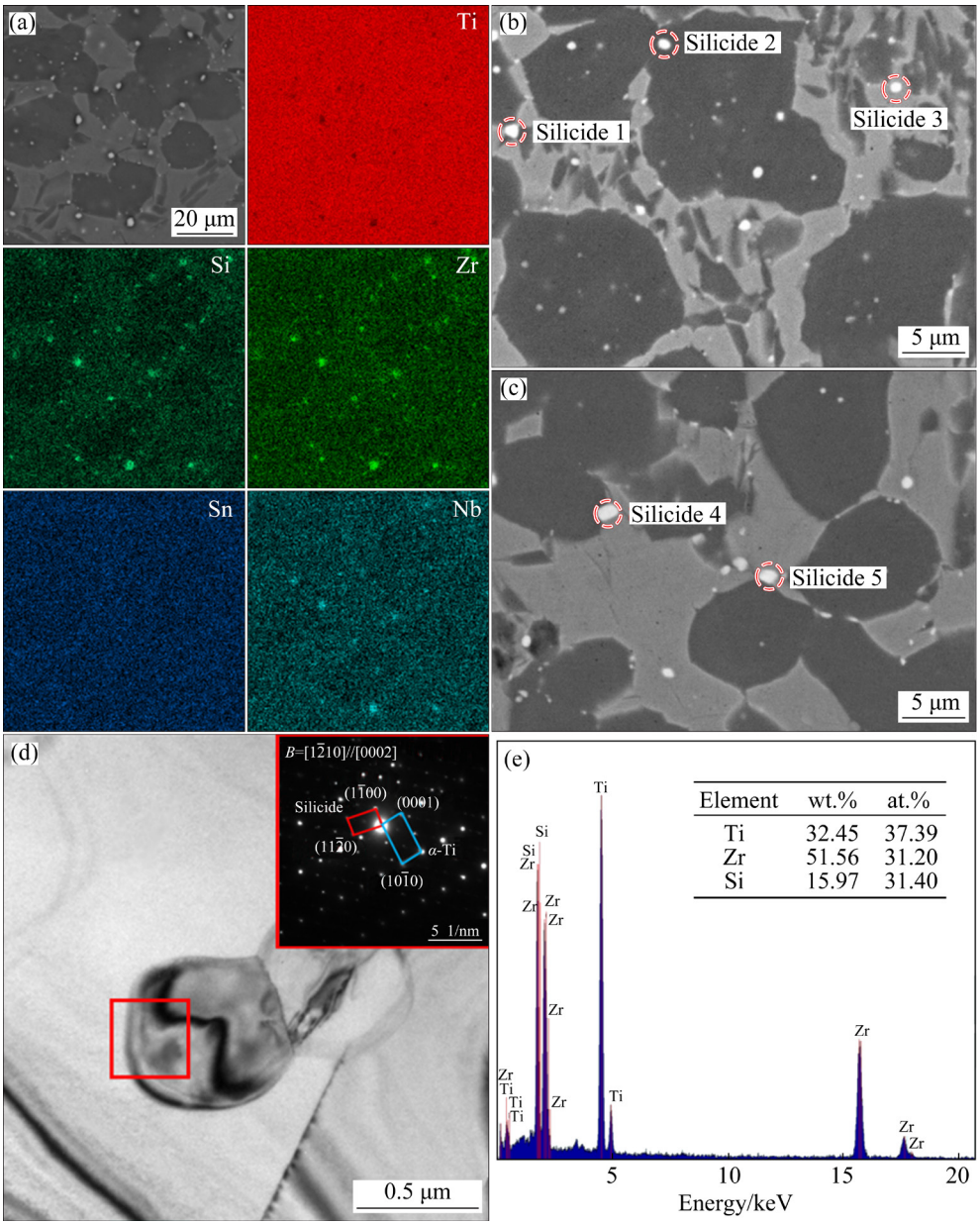

Fig. 3 Silicide precipitation analyses of Ti65 alloy ultrathin sheet samples after solution treatments followed by air cooling: (a) Elemental mapping images of Ti, Si, Zr, Sn and Nb in 950 ℃-2 h-AC sample; Selected silicides for element analyses in 950 ℃-0.25 h-AC sample (b) and 950 ℃-2 h-AC sample (c); TEM image and corresponding SAED pattern of 950 ℃-24 h-AC sample (d); (e) Corresponding EDS results of selected silicide in (d)

Table 2 Elemental composition of selected silicides during spot scanning

Silicide No.	Composition/at.%			(Ti,Zr)/Si	Ti/Zr
	Ti	Zr	Si		
1	25.1	11.27	12.11	3	2.23
2	13.55	8.93	10.7	2.1	1.51
4	23.44	10.43	11.55	2.93	2.25
4	27.52	12.77	15.08	2.67	2.16
5	26.71	14.64	16.19	2.55	1.82

Table 3 Tensile properties of Ti65 alloy ultrathin sheet samples after air cooling at ambient temperature

Sample	UTS/MPa	TYS/MPa	EL/%
As-rolled	1117.99±3.68	1003.64±6.89	11.75±0.75
950 ℃-0.25 h-AC	1049.43±1.60	978.84±30.00	6.40±3.40

(EL) of the as-rolled sample, i.e., 1117.99 MPa, 1003.64 MPa and 11.75%, are all higher than those of the 950 ℃-0.25 h-AC sample, i.e., 1049.43 MPa,

978.84 MPa and (6.40±3.40)%. Obviously, the weak precipitation strengthening effect generated by submicron silicides in the current work cannot compensate for the diminished solid solution strengthening effect. Additionally, great performance fluctuations in elongation in the 950 ℃-0.25 h-AC sample are observed as a result of the combined effect of the size effect and silicide precipitation.

Further analyses are carried out according to the true stress−strain curves and fracture morphology images in Fig. 4. Ductile fracture morphology is observed in the as-rolled sample (Fig. 4(c)), including many deep dimples and a few tearing edges. However, the dimples become increasingly shallower and smaller due to silicide precipitation (Fig. 4(d)). Generally, $(Ti,Zr)_6Si_3$ silicide hinders dislocation movement owing to no coherent connection with the matrix [21,22]. The resulting dislocation accumulation causes a strong stress concentration, which leads to an earlier yield stage (Fig. 4(b)) and a lower TYS in the 950 ℃-0.25 h-AC sample. Meanwhile, due to the lack of dislocations for the growth of dimples, more dimples have to be produced to coordinate deformation, even if the new dimples are shallow and small. Consequently, the loss of tensile properties occurs after silicide precipitation.

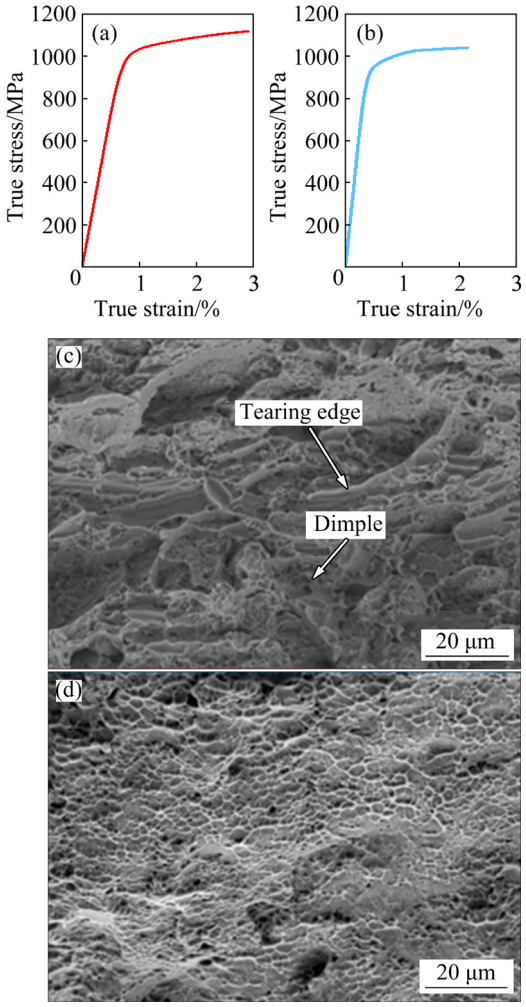

Fig. 4 True stress−strain curves (a, b) and fracture morphology images (c, d) of as-rolled (a, c) and 950 ℃-0.25 h-AC (b, d) samples

3.1.3 Novel $\{10\bar{1}1\}$ twinning

A small amount of twinning is observed, but only inside equiaxed α phases. The matrix α grains are all large and show similar red colours, which may favour twinning system activation. The twinning remains even after solution treatment at 950 ℃ for 8 h, indicating high thermal stability. Three grains marked in Fig. 5 are selected for analyses. The lines shown in the morphology images (Fig. 6) are related to point-to-origin misorientation diagrams, in which the circle represents the initiation point and the direction indicated by the arrow represents the position of the subsequent point. The axis−angle pair of the twinning system acquired by Channel 5 software is concluded to be $65°\langle 8\bar{4}\bar{4}3\rangle$, which varies from previous studies. IPFs of matrix α grains are displayed. The c axis of all matrix α grains is close to the normal direction, showing that matrix α

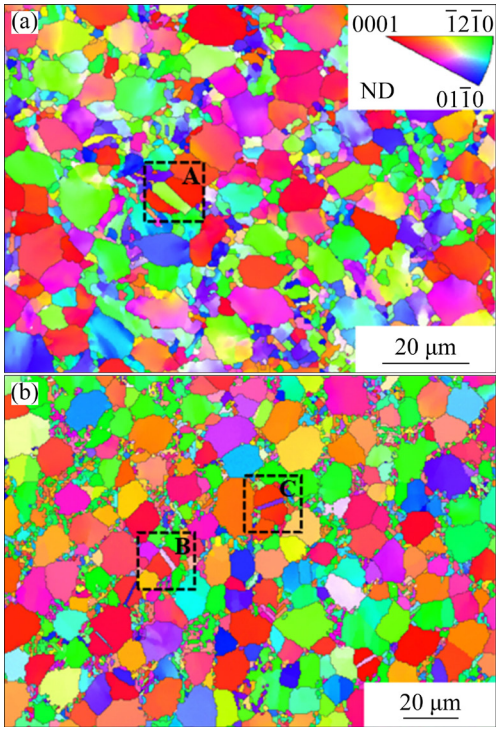

Fig. 5 Inverse pole figure maps of Ti65 alloy ultrathin sheet samples after air cooling: (a) As-rolled; (b) 950 ℃-8 h-AC

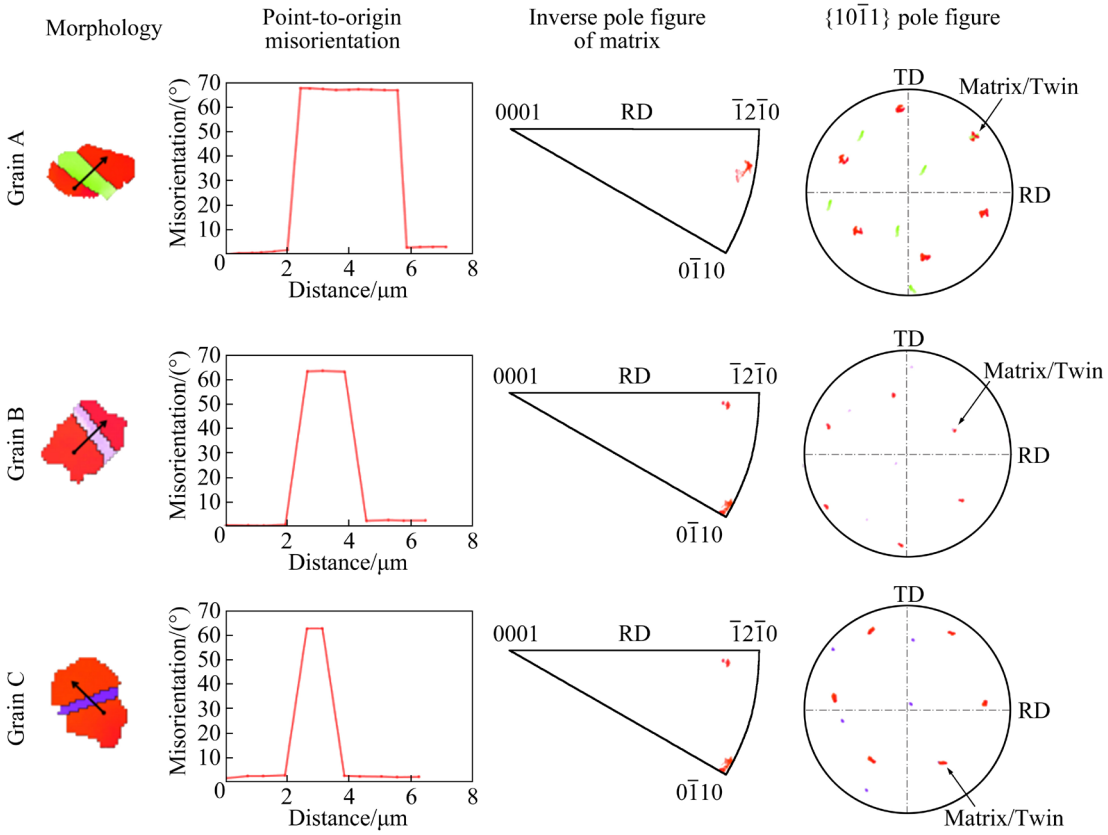

Fig. 6 EBSD analyses of grains marked in Fig. 5 (The lines shown on the morphology images are related to point-to-origin misorientation diagrams, in which the circle represents the origin and the direction indicated by the arrow represents the position of subsequent points; The characteristic direction of the inverse pole figure of the matrix is RD; The scattered points where the matrix and twinning coincide on the {10$\bar{1}$1} pole diagram are indicated by arrows)

grains have a basal texture. The scattered points where the matrix and twin coincide on the {10$\bar{1}$1} pole diagram of all three grains are indicated by arrows. However, the pole figure shows the orientation relationship only in two-dimensional space. Although the matrix grain and the twinning share parallel {10$\bar{1}$1} planes, it is not accurate enough to identify the twinning system.

The FIB technique was applied to preparing an accurately cut sample, and the sample position is marked by a green box in Fig. 7(a). The FIB lifted-out lamellar sample from the 950 °C-4 h-AC sample was subjected to TEM analyses. Black and white spaced stripes are observed in the corresponding BF image due to crystal orientation differences. The SAED pattern taken from the region marked by the yellow box is shown in Fig. 7(d). There are two groups of diffraction spots. One of them is clearly visible and corresponds to the matrix grain. Simultaneously, the fuzzy one is circled in red. The dark field image (Fig. 7(f)) indicates that it is resulted from twinning. The two groups of diffraction spots are mirror symmetric and share a common $(01\bar{1}1)_{\alpha}$ plane, indicating novel type {10$\bar{1}$1} twinning.

3.2 Solution treatments followed by furnace cooling

3.2.1 Coexistence of silicides

The solution treatments at four different temperatures followed by furnace cooling were applied to studying silicide precipitation. The micrographs shown in Fig. 8 indicate similar equiaxed structures between the four samples. However, as the solution temperature rises, the α grain size grows quickly, and the volume fraction of lamellar α also increases slightly. Silicide precipitation occurs in each case but varies. The volume fraction of silicides decreases with increasing solution temperature, while the size of silicides increases slightly.

TEM characterizations of the 950 °C-2 h-FC sample are displayed in Figs. 9(a_1, a_2). $(Ti,Zr)_6Si_3$ silicide with a typical ellipsoidal morphology is

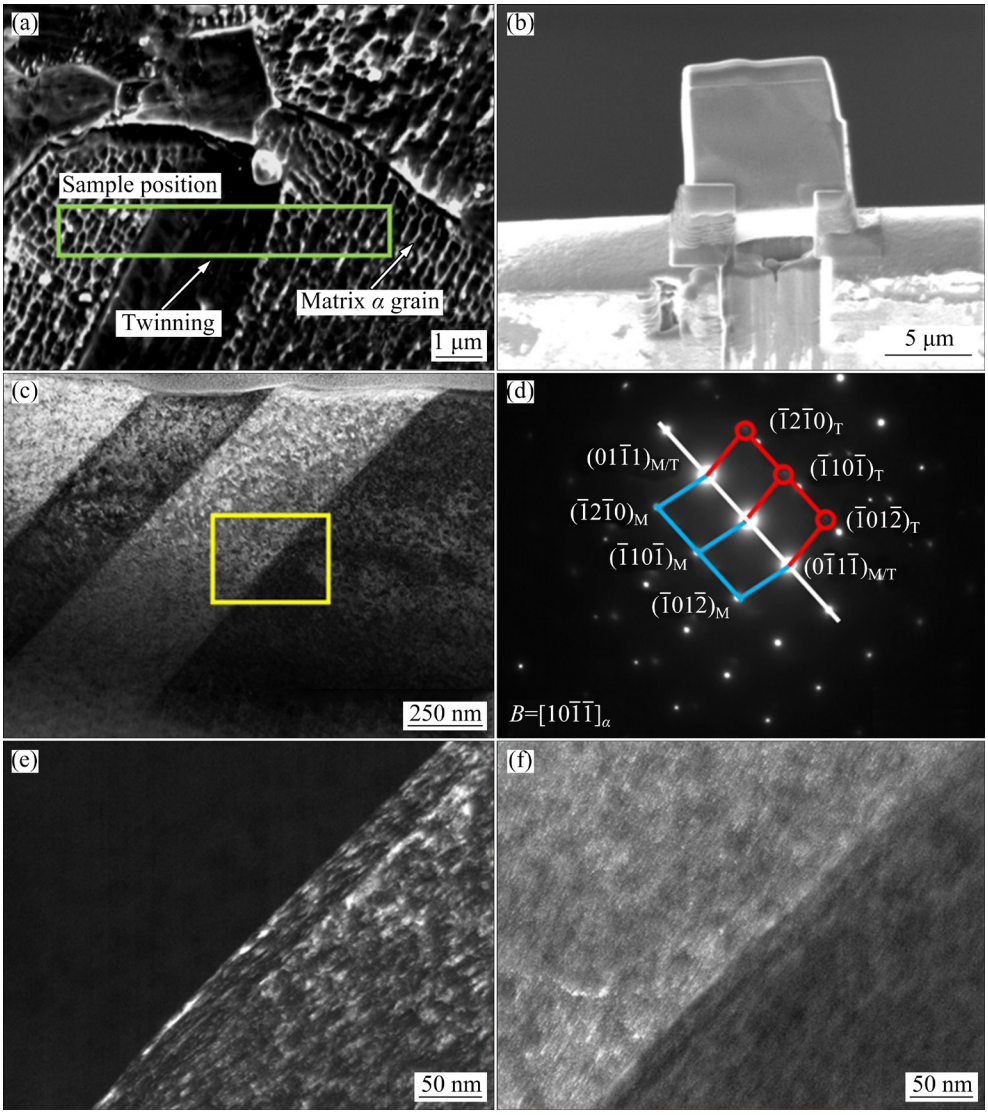

Fig. 7 TEM analyses of 950 ℃-4 h-AC sample: (a) Sample position of FIB; (b) FIB lifted-out lamella sample; (c) BF image of FIB sample; (d) Corresponding SAED pattern taken from region marked in (c); (e, f) DF images of matrix (e) and twinning (f) spots

distributed near the grain boundaries. Furthermore, there is a new silicide crossing the grain boundaries, confirmed as $(Ti,Zr)_5Si_3$. As mentioned above, the two kinds of silicides precipitate during the low- and high-temperature ageing processes. The coexistence phenomenon should be correlated with the characteristics of furnace cooling. A similar coexistence phenomenon occurs when the solution temperature rises to 1010 ℃ (Figs. 9(b_1, b_2)). However, an unexpected silicide is observed near dislocations (Fig. 9(b_3)) but in small quantities. Based on the typical tetragonal lattice SAED pattern and zirconium confirmed by the EDS result in Fig. 9(c), the unexpected silicide is determined to be $(Ti,Zr)_3Si$.

Table 4 summarizes the tensile properties of the furnace cooling samples. In comparison to the as-rolled sample, a sharp drop in EL occurs in the 950 ℃-2 h-FC sample (from 11.75% to 2.67%). Simultaneously, the UTS and TYS values decrease from 1003.61 and 1117.99 MPa to 934.32 and 937.67 MPa, respectively. Numerous shallow dimples are observed in Fig. 10(c), and silicides are distributed at the bottom of the dimples, which is similar to the fracture morphology of 950 ℃-0.25 h-AC sample. A severe drop in EL occurs again after the solution temperature rises to 1010 ℃. The absence of yield stage can be seen from the true stress−strain curve (Fig. 10(b)). Its EL is 0%, as the result of brittle fracture. The breaking strength is

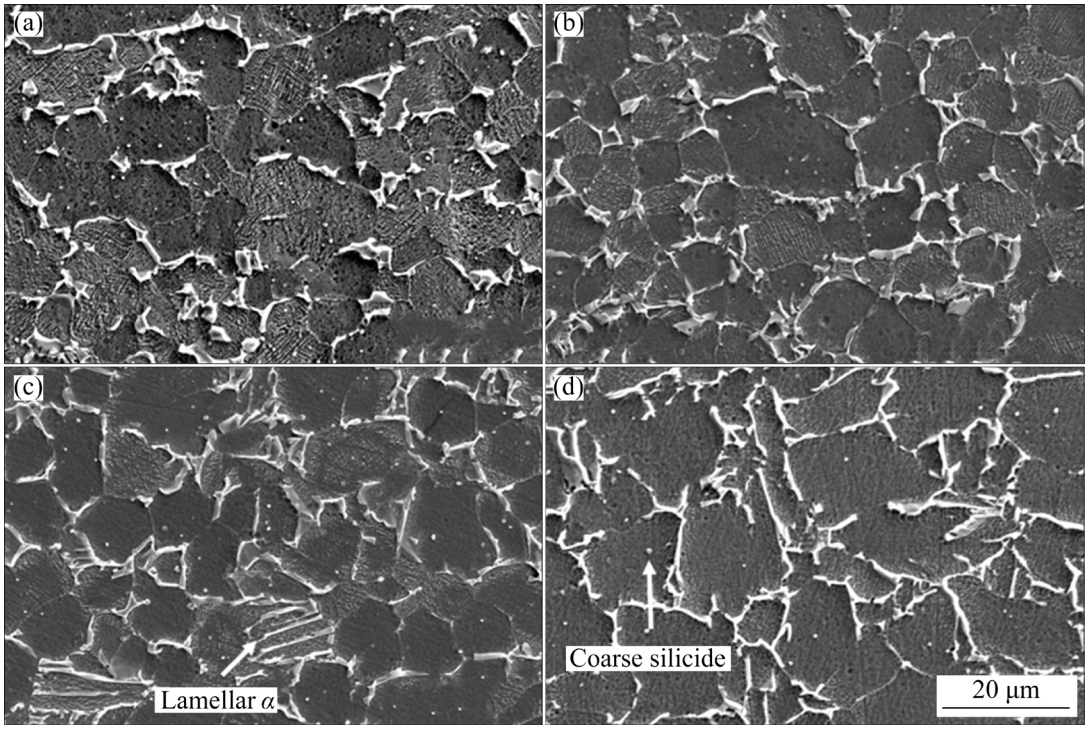

Fig. 8 Micrographs of Ti65 alloy ultrathin sheet samples after solution treatments followed by furnace cooling: (a) 950 ℃-2 h-FC; (b) 970 ℃-2 h-FC; (c) 990 ℃-2 h-FC; (d) 1010 ℃-2 h-FC

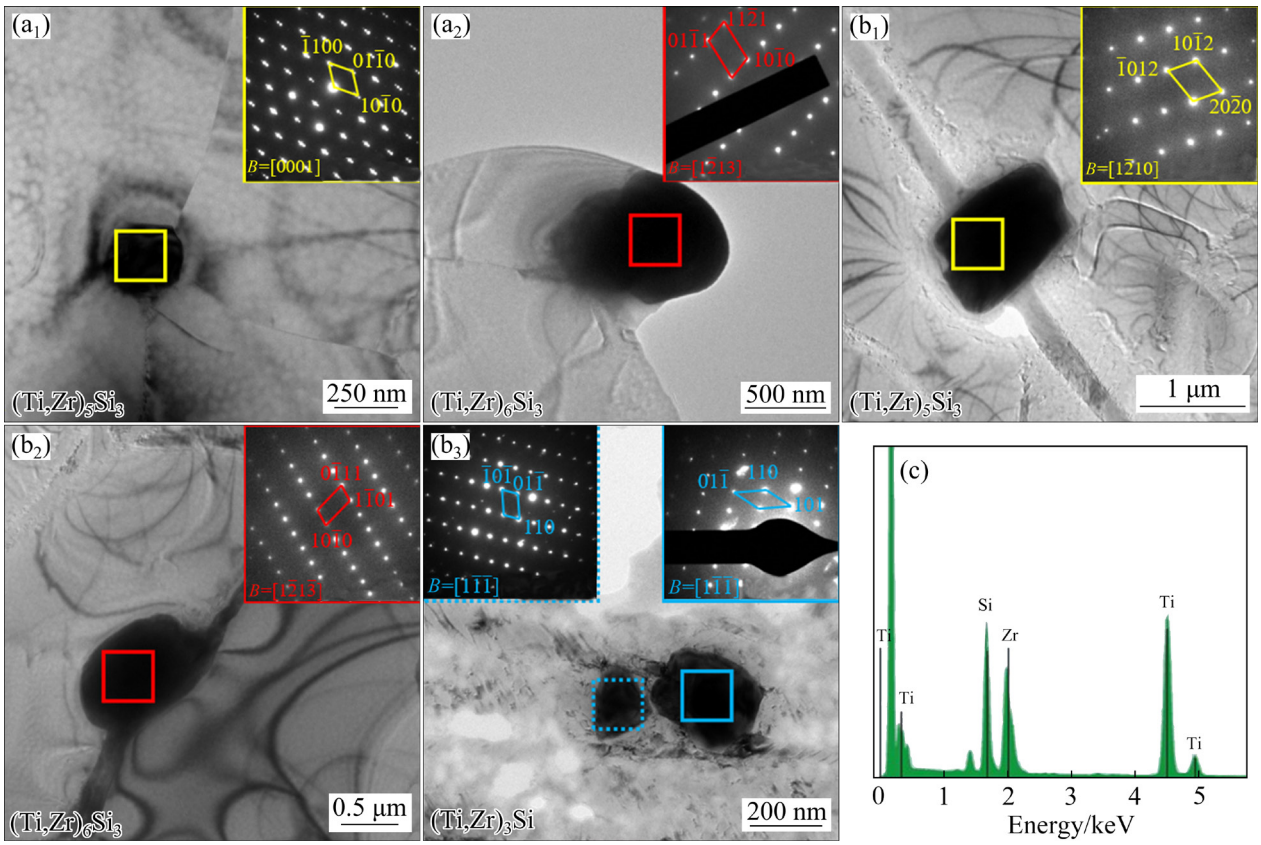

Fig. 9 TEM images showing silicide precipitation in Ti65 alloy ultrathin sheet samples after solution treatments followed by furnace cooling: (a_1, a_2) $(Ti,Zr)_5Si_3$ and $(Ti,Zr)_6Si_3$ in 950 ℃-2 h-FC sample; (b_1, b_2, b_3) $(Ti,Zr)_5Si_3$, $(Ti,Zr)_6Si_3$ and $(Ti,Zr)_3Si$ in 1010 ℃-2 h-FC sample; (c) EDS result of large silicide shown in (b_3)

Table 4 Tensile properties of Ti65 alloy ultrathin sheet samples after furnace cooling at ambient temperature

Samlple	UTS/MPa	TYS/MPa	EL/%
950 ℃-2 h-FC	937.67±9.33	934.32±3.68	2.67±0.67
1010 ℃-2 h-FC	(858.65±80.38)*		0

* Breaking strength

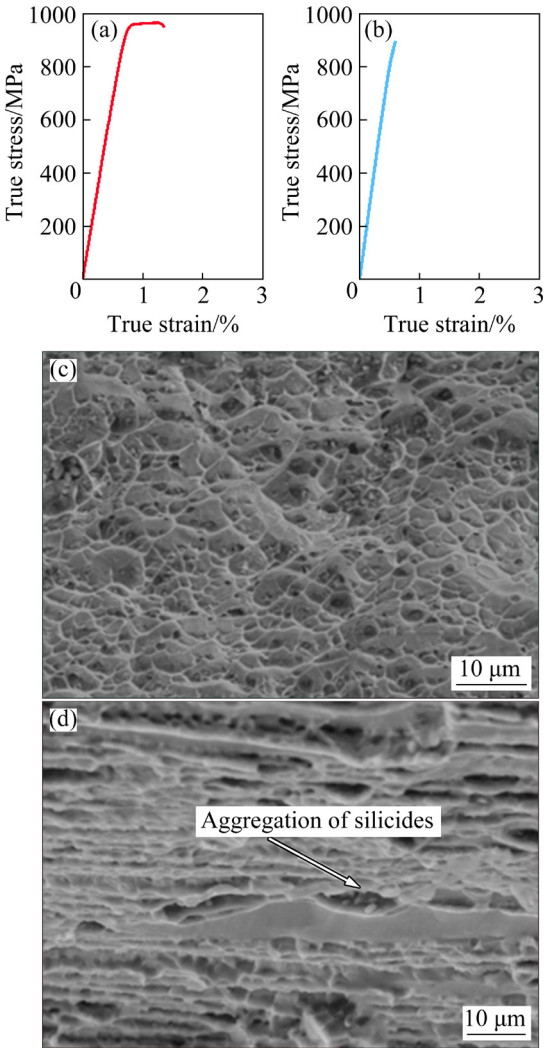

Fig. 10 True stress−strain curves (a, b) and fracture morphology images (c, d) of 950 ℃-2 h-FC (a, c) and 1010 ℃-2 h-FC (b, d) samples

858.65 MPa, but with a huge fluctuation of 80.38 MPa in the value. Many silicides aggregate between tearing edges (Fig. 10(d)), which can promote the initiation of large voids. Clearly, the prominent size effect produced by α grain growth leads to greater degradation of mechanical properties with the assistance of silicides.

3.2.2 Growth of silicides

Due to the difficulties in controlling the microstructure and α grain size, solution treatments at 950 ℃ rather than at higher temperatures are applied to study the effect of holding time on silicide precipitation. Silicide diameter distribution map in Fig. 11 and quantitative statistics in Table 5 provide a reference for studying the evolution of silicide precipitation. Similar silicide diameter distributions are observed in the three samples, but the deviation of the silicide diameter decreases slightly and then increases with increasing holding time. The volume fraction of silicides ranges from 0.55% to 0.58%. However, the slight change in silicides is negligible compared to the significant increase in holding time. In conclusion, the effect of holding time on silicide precipitation is weak during low-temperature solution treatments followed by furnace cooling.

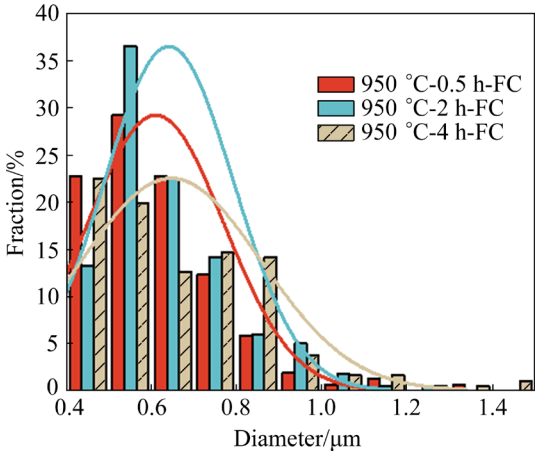

Fig. 11 Silicide diameter distributions of Ti65 alloy ultrathin sheet samples after furnace cooling

Table 5 Quantitative statistics of silicide in Ti65 alloy ultrathin sheet samples after furnace cooling

Sample	Area fraction/%	D_{max}/μm	D_{min}/μm	Weighted mean/μm	Deviation/μm
950 ℃-0.5 h-FC	0.58	1.37	0.32	0.61	0.16
950 ℃-2 h-FC	0.58	1.21	0.42	0.63	0.15
950 ℃-4 h-FC	0.55	1.43	0.36	0.64	0.21

4 Discussion

4.1 Silicide precipitation mechanism

In the case of Ti−Zr−Si ternary system alloys, $(Ti,Zr)_5Si_3$ silicide is advantageously allocated, which is also denoted as S1-type in the literature [23,24]. Zirconium shows the same chemical valence as Ti, with zirconium solubility in

Ti_5Si_3 reaching 9 at.%, which promotes the partial replacement of titanium atoms with zirconium atoms [25]. Zirconium can reduce the high strain energy caused by structure mismatch between the α phase and silicide and reduce the activation nucleation energy of silicides [10]. Generally, the zirconium enrichment of $(Ti,Zr)_5Si_3$ silicide promotes the transformation to $(Ti,Zr)_6Si_3$ (S2-type) silicide [26] as the heat treatment time increases.

For air cooling samples, silicide precipitation should be related to the inherent characteristics of ultrathin sheets. YUE et al [18] reported no silicide precipitation in a 1019 ℃-2 h-AC sample of Ti65 bars. Silicide dissolution occurs when the heating treatment temperature is higher than the silicide dissolution temperature. However, specific data on the silicide dissolution temperature of Ti65 alloy could not be obtained from previous studies. For reference, the silicide dissolution temperature of the near α titanium alloy Ti600 (Ti−Al−Sn−Zr−Mo−Si) is applied, which is 20 ℃ higher than the β transformation temperature of 1010 ℃ [27]. Hence, the occurrence of silicide precipitation is not temperature-dependent but related to the difference in cooling rate between bars and ultrathin sheets. Silicide can be preserved after solution treatments followed by water quenching. With ultrathin thickness, air cooling samples in the present work cool at a faster rate, which causes silicide precipitation after air cooling. However, for bars, slow heat conduction leads to good internal heat preservation. Hence, no silicide precipitation occurs in the bar after air cooling due to the slow cooling speed.

For furnace cooling samples, the coexistence phenomenon should be related to the characteristics of furnace cooling. Due to the slow cooling speed, the furnace cooling process can be regarded as an ageing process with a continuous temperature drop. When the heating temperature is 950 ℃, $(Ti,Zr)_6Si_3$ silicide precipitation occurs during the early stage of the cooling process. Owing to the high driving force at high temperature, $(Ti,Zr)_6Si_3$ silicide precipitation can occur in areas with relatively small element solubility differences. When the cooling temperature drops, a slow cooling speed results in a long time duration. There is enough time for element diffusion and subsequent silicide precipitation. However, due to the lack of driving force at low temperature, only in the regions where element solubility varies greatly can $(Ti,Zr)_5Si_3$ silicide precipitate. In this way, $(Ti,Zr)_5Si_3$ silicide crossing the grain boundaries and $(Ti,Zr)_6Si_3$ silicide near the grain boundaries are observed. Furthermore, when the initial cooling temperature rises to 1010 ℃, more β-Ti phases exist according to the lever rule. Based on the accepted Ti−Si phase diagram, Ti_3Si silicide can be obtained at high temperature by the peritectoid reaction [28]:

$$\beta\text{-Ti}+Ti_5Si_3 \rightleftharpoons Ti_3Si \quad (1)$$

Silicon in titanium appears in two states: solid solution state and precipitation state. The distribution of solid solution silicon is not uniform. For instance, the segregation of silicon is more likely to occur around dislocations and other crystal defects [29], which may promote $(Ti,Zr)_5Si_3$ silicide precipitation near dislocations with the help of many β phases. Thus, a few $(Ti,Zr)_3Si$ can be observed near dislocations after high-temperature solution treatment followed by furnace cooling.

4.2 Novel {10$\bar{1}$1} twinning system activation mechanism

Six common twinning systems in α titanium are listed in Table 6. The axis−angel pair of the normal $\{10\bar{1}1\}$ twinning system, $57.3°\langle 1\bar{2}10\rangle$, differs from that of the $\{10\bar{1}1\}$ twinning system in our work, $65°\langle 8\bar{4}\bar{4}3\rangle$. In brief, the $\{10\bar{1}1\}$ twinning system with an axis−angle pair of $65°\langle 8\bar{4}\bar{4}3\rangle$ is called the novel $\{10\bar{1}1\}$ twinning system. CHRISTIAN and MAHAJAN [31] suggested that the favourable conditions for twinning system activation are low twinning shear and a small extent of atomic shuffling. The low twinning shear of the normal $\{10\bar{1}1\}$ twinning system favours twinning activation at high temperatures. However, based on previous studies,

Table 6 Six common twinning systems in α titanium [30]

Twinning system	Axis−angle pair	Twinning shear	Remark
$\{10\bar{1}2\}\langle 10\bar{1}\bar{1}\rangle$	$84.7°\langle 1\bar{2}10\rangle$	0.167	Tensile twin
$\{11\bar{2}1\}\langle 11\bar{2}\bar{6}\rangle$	$35.1°\langle \bar{1}100\rangle$	0.638	
$\{11\bar{2}3\}\langle 33\bar{6}2\rangle$	$87.3°\langle \bar{1}100\rangle$	0.533	
$\{10\bar{1}1\}\langle 10\bar{1}2\rangle$	$57.3°\langle 1\bar{2}10\rangle$	0.105	Compressive twin
$\{11\bar{2}2\}\langle 11\bar{2}\bar{3}\rangle$	$64.6°\langle \bar{1}100\rangle$	0.225	
$\{11\bar{2}4\}\langle 11\bar{2}1\rangle$	$77.2°\langle \bar{1}100\rangle$	0.254	

the normal $\{10\bar{1}1\}$ twinning system is activated only at 400−800 ℃. The rolling temperature applied in our work is 990 ℃, which is much higher. To summarize, the novel $\{10\bar{1}1\}$ twinning system should show much lower twinning shear.

As is well known, twinning system activation is affected by grain size. The smaller the α grain size is, the more difficult it is for the twinning system to be activated [32]. A long slip distance in coarse grains leads to strong dislocation pile-up near grain boundaries, and the resulting stress concentration promotes twinning system activation. In contrast, the short slip distance and high volume fraction of grain boundaries in fine grains weaken the stress concentration [33]. The small average α grain size in the Ti65 alloy ultrathin sheet inhibits twinning system activation, while there are a small amount of large basal texture α grains. STAPLETON et al [34] reported that basal texture α grains accumulate significantly less residual lattice strain. Simultaneously, the α phase with low residual lattice strain is less likely to transform to the β phase. Therefore, basal texture α grains grow quickly during heating, which favours twinning system activation.

However, the Schmid factor (SF) value of the normal $\{10\bar{1}1\}$ twinning system in basal texture α grains during the rolling process is not high. The SF value is calculated according to the following: the ultrathin sheet is subjected to tensile stress along RD and compressive stress along ND. Values of the two stresses are assumed to be equal. Since the loading direction of compressive stress is opposite to that of tensile stress, the value of compressive stress is negative. The calculation formula of SF (m) is

$$m=0.5(\cos\alpha\cdot\cos\beta-\cos\gamma\cdot\cos\delta) \quad (2)$$

where α represents the included angle between the loading direction of tensile stress and the slip direction, and β corresponds to the included angle between the loading direction of tensile stress and the normal direction of the slip plane. Similarly, γ and δ represent the included angles between the loading direction of compressive stress and the slip direction as well as the normal direction of the slip plane, respectively.

The crystal orientations expressed by Euler angle $\{\varphi_1, \Phi, \varphi_2\}$ of the three grains marked in Fig. 5 are {155°, 8°, 5°} (Grain A), {137°, 160°, 46°} (grain B) and {174°, 14°, 5°} (Grain C). The highest SF value is 0.26, and the corresponding normal $\{10\bar{1}1\}$ twinning system variant is $(1\bar{1}0\bar{1})$-$[1\bar{1}0\bar{2}]$. The low SF value of the normal $\{10\bar{1}1\}$ twin indicates large difficulty of twinning system activation. However, with different twinning directions, it is possible for the novel $\{10\bar{1}1\}$ twinning system to show a high SF value for basal texture α grains.

Various substitution elements of the Ti65 alloy favour novel $\{10\bar{1}1\}$ twinning system activation. The relationship between twinning boundary energy (γ_{TBE}) and stacking fault energy (γ_{SFE}) is defined as follows [35]:

$$\gamma_{TBE}=(0.5-0.75)\gamma_{SFE} \quad (3)$$

Previous studies on FCC alloys suggested that the addition of substitutional atoms reduces the stacking fault energy [36], which promotes twinning system activation. Similar conclusions were drawn by studies on HCP alloys. FITZNER et al [37] proposed that raising the aluminium content in titanium can slightly enhance twinning system activation. As noted above, the Ti65 alloy (Ti−Al−Sn−Zr−Mo−Si−Nb−Ta−W−C) is a ten-component alloy. Various substitution elements result in a great drop in stacking fault energy; thus, novel $\{10\bar{1}1\}$ twinning system activation arises in Ti65 alloy ultrathin sheets in the present work.

4.3 Mechanical behaviour under size effect and silicide precipitation

When the thickness of the samples is close to the magnitude of the polycrystalline microstructure, the so-called size effect can induce dramatic changes in the mechanical properties of titanium alloy sheets. Three theories, the surface model [38], grain boundary strengthening effect [39] and oxide layer strengthening effect [40], are applied to explain the mechanism of the size effect. In brief, the size effect enhances the contribution of individual grain to the overall mechanical properties, which promotes the formation of an easy deformation zone. After loading, grains called soft orientation grains are prone to deform due to the favourable crystal orientation, and they consume minimum plastic work during deformation [41]. Meanwhile, other grains that are difficult to deform are called hard orientation grains. The assumption that samples deform along the path on which

grains consume minimum plastic work is applied for the following analyses [42]. In the case of polycrystalline samples, the minimum plastic work consumption is more likely to be achieved through the combination of soft orientation grains. As shown in Fig. 12(a), the combination is a so-called easy-deformation-zone. Generally, the formation of an easy-deformation-zone results in massive concentrated plastic work. Hence, local stress can easily reach fracture strength, and premature fracture and deterioration of mechanical properties follow. In comparison to sheets and bars, there are fewer grains along the thickness direction in ultrathin sheets with the same α grain size. In other words, the formation of an easy-deformation-zone occurs more frequently in ultrathin sheets.

High, medium and low T/D ratios can be achieved in 950 ℃-0.25 h-AC, 950 ℃-2 h-FC and 1010 ℃-2 h-FC samples, respectively, where T represents the thickness and D is the diameter of the α grain. The mechanical behaviour under the size effect and silicide precipitation varies according to the T/D ratio. In the case of the high T/D ratio samples (Fig. 12(b)), it is difficult for an easy-deformation-zone to form due to hundreds of grains along the thickness direction. In other words, silicides are widely distributed outside the easy-deformation-zone in most cases. Although the strong stress concentration caused by silicide precipitation can further enhance the local stress concentration in the easy-deformation-zone, if the number of silicides in the easy-deformation-zone does not reach a certain threshold, only a slight drop in elongation occurs. In contrast, if silicide precipitation in the easy-deformation-zone is sufficient to cause a significant local stress concentration, a sharp drop in ductility occurs, such as a 3.00% elongation of 950 ℃-0.25 h-AC sample. Consequently, a large fluctuation in the elongation of 950 ℃-0.25 h-AC sample is observed.

For the medium T/D ratio samples (Fig. 12(c)), the growth of α grains indicates fewer grains along the thickness direction, indicating that an easy-deformation-zone is prone to form. Even with fewer silicides, the volume fraction of silicides in the easy-deformation-zone increases significantly; hence, a strong local stress concentration takes place. Moreover, coarse α grains contribute to harder compatible deformation among α grains. Therefore, a sharp drop in elongation rather than performance fluctuation occurs in the 950 ℃-2 h-FC sample.

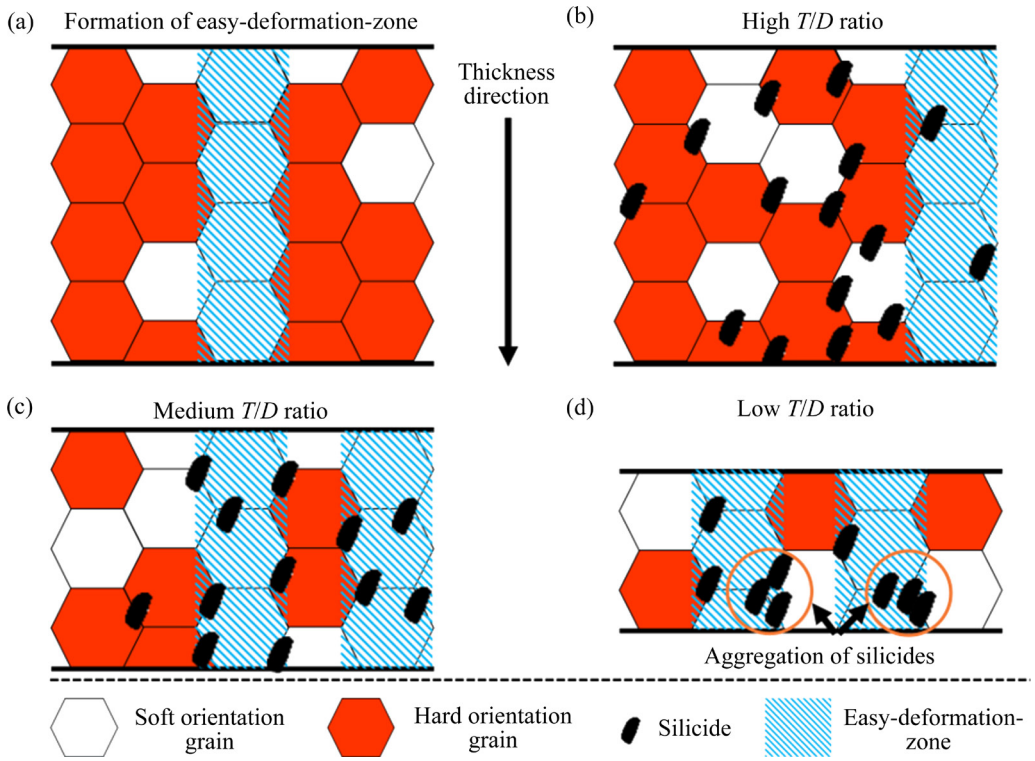

Fig. 12 Schematic showing formation of easy-deformation-zone (a) and distribution relationship between silicides and easy-deformation-zone of heat-treated samples with different T/D ratios (b−d)

When the *T*/*D* ratio drops to a low value (Fig. 12(d)), there is no doubt that the volume fraction of silicides in the easy-deformation-zone is higher and that compatible deformation between the *α* grains is more difficult, which will lead to further deterioration of the mechanical properties. In addition, the volume fraction of grain boundaries decreases notably. Due to fewer nucleate particles, silicides precipitate and aggregate. The aggregation of silicides can act as the initiation of large voids. Accordingly, brittle fracture rather than ductile fracture takes place after the tensile test of the 1010 ℃-2 h-FC sample.

5 Conclusions

(1) For air cooling samples, the submicron silicide is deduced to be $(Ti,Zr)_6Si_3$. The following orientational correlation between silicide and the matrix is identified: $[1\bar{2}10]_{\alpha\text{-Ti}} // [0002]_{\text{Silicide}}$ and $(10\bar{1}1)_{\alpha\text{-Ti}} // (\bar{3}120)_{\text{Silicide}}$. After silicide precipitation, the UTS decreases by 24.80 MPa (from 1003.64 to 978.84 MPa), and decrease and fluctuation of EL occur.

(2) For furnace cooling samples, different solution temperatures result in various silicide precipitates. After 950 ℃ solution treatment, $(Ti,Zr)_5Si_3$ silicide crossing the grain boundaries and $(Ti,Zr)_6Si_3$ silicide near the grain boundaries are observed. When the temperature rises further to 1010 ℃, the third silicide $(Ti,Zr)_3Si$ appears near dislocations. Significant deterioration in tensile properties is observed for the furnace cooling samples, and brittle fracture even takes place in the 1010 ℃-2 h-FC sample. In addition, silicide precipitation differs little with various holding time during low-temperature solution followed by furnace cooling.

(3) The mechanical behaviour under the size effect and silicide precipitation varies according to the *T*/*D* ratio. Ultrathin thickness and *α* grain growth promote the formation of an easy-deformation-zone. The silicide precipitation in the easy-deformation-zone further aggravates the local stress concentration. When the *T*/*D* ratio decreases, a higher volume fraction of silicides in the easy-deformation-zone and harder compatible deformation among *α* grains lead to more serious deterioration of the mechanical properties. Consequently, great performance fluctuation, a sharp drop in tensile properties and even brittle fracture take place.

(4) The novel $\{10\bar{1}1\}$ twinning appears only inside coarse basal texture *α* grains in Ti65 alloy ultrathin sheets rolled at 990 ℃, with axis−angle pair of $65°\langle 8\bar{4}\bar{4}3\rangle$.

Acknowledgments

The authors gratefully acknowledge the National Natural Science Foundation of China (Nos. 51801156 and 52074231) and the Chongqing Natural Science Foundation, China (No. cstc2020jcyj-msxmX1056) for the financial support to this work.

References

[1] LIU Na, WANG Ying, HE Wei-jun, LI Jun, CHAPUIS A, LUAN Bai-feng, LIU Qing. Microstructure and textural evolution during cold rolling and annealing of commercially pure titanium sheet [J]. Transactions of Nonferrous Metals Society of China, 2018, 28(6): 1123−1131.

[2] LI Jin-shan, DONG Rui-feng, KOU Hong-chao, FAN Jiang-kun, ZHU Bin, TANG Bin. Texture evolution and the recrystallization behavior in a near *β* titanium alloy Ti-7333 during the hot-rolling process [J]. Materials Characterization, 2020, 159: 109999.

[3] MA Zhen-wu, TONG G Q, CHEN Feng, WANG Qi, WANG Shi-chuan. Grain size effect on springback behavior in bending of Ti−2.5Al−1.5Mn foils [J]. Journal of Materials Processing Tech, 2015, 224: 11−17.

[4] ELSHAER R N, IBRAHIM K M. Effect of cold deformation and heat treatment on microstructure and mechanical properties of TC21 Ti alloy [J]. Transactions of Nonferrous Metals Society of China, 2020, 30(5): 1290−1299.

[5] ZHANG Zhi-xin, FAN Jiang-kun, TANG Bing, KOU Hong-chao, WANG Jian, WANG Xin, WANG Shi-ying, WANG Qing-jiang, CHEN Zhi-yong, LI Jin-shan. Microstructural evolution and FCC twinning behavior during hot deformation of high temperature titanium alloy Ti65 [J]. Journal of Materials Science & Technology, 2020, 49: 56−69.

[6] HUANG Z W, YONG P L, ZHOU H, LI Y S. Grain size effect on deformation mechanisms and mechanical properties of titanium [J]. Materials Science and Engineering A, 2020, 773: 138721.

[7] NIE Da-ming, LU Zhen, ZHANG Kai-feng. Grain size effect of commercial pure titanium foils on mechanical properties, fracture behaviors and constitutive models [J]. Journal of Materials Engineering and Performance, 2017, 26(3): 1283−1292.

[8] WANG Qing-jiang, LIU Jian-rong, YANG Rui. High temperature titanium alloys status and perspective [J]. Journal of Aeronautical Materials, 2014, 34(4): 1−26.

[9] TAVARES A M G, RAMOS W S, de BLAS J C G, LOPES E S N, CARAM R, BATISTA W W, SOUZA S A. Influence of

Si addition on the microstructure and mechanical properties of Ti−35Nb alloy for applications in orthopedic implants [J]. Journal of the Mechanical Behavior of Biomedical Materials, 2015, 51: 74−87.

[10] LI juan, CAI Jian-ming, DUAN Rui. Precipitation behavior of silicide in near-α TG6 titanium alloy [J]. Journal of Aeronautical Materials, 2012, 32(5): 32−36.

[11] ZHANG Zhi-xin, FAN Jiang-kun, WU Zhi-yong, ZHAO Ding, GAO Qi, WANG Qin-bo, CHEN Zhi-yong, TANG Bing, KOU Hong-chao, LI Jin-shan. Precipitation behavior and strengthening−toughening mechanism of hot rolled sheet of Ti65 titanium alloy during aging process [J]. Journal of Alloys and Compounds, 2020, 831: 154786.

[12] ZHANG Wen-jing, SONG Xiao-yun, HUI Song-xiao, YE Wen-jun. Phase precipitation behavior and tensile property of a Ti−Al−Sn−Zr−Mo−Nb−W−Si titanium alloy [J]. Rare Metals, 2018, 37(12): 1064−1069.

[13] SRINADH K V S, SINGH N, SINGH V. Role of Ti 3 Al/silicides on tensile properties of Timetal 834 at various temperatures [J]. Bulletin of Materials Science, 2007, 30(6): 595−600.

[14] WANG Qing-qing. Investigations on the microstructure formation and evolutions during machining of Ti−6Al−4V [D]. Jinan, China: Shandong University, 2019.

[15] ZHONG H Z, ZHANG X Y, WANG S X, GU J F. Examination of the twinning activity in additively manufactured Ti−6Al−4V [J]. Materials & Design, 2018, 144: 14−24.

[16] PATON N E, BACKOFEN W A. Plastic deformation of titanium at elevated temperatures [J]. Metallurgical Transactions, 1970, 1(10): 2839−2847.

[17] ZENG Zhi-peng, JONSSON S, ROVEN H J. The effects of deformation conditions on microstructure and texture of commercially pure Ti [J]. Acta Materialia, 2009, 57: 5822−5833.

[18] YUE Ke, LIU Jian-rong, ZHANG Hai-jun, YU Hui, SONG Yuan-yuan, HU Qing-miao, WANG Qing-jiang, YANG Rui. Precipitates and alloying elements distribution in near α titanium alloy Ti65 [J]. Journal of Materials Science & Technology, 2020, 36: 91−96.

[19] SALPADORU N H, FLOWER H M. Phase equilibria and transformations in a Ti−Zr−Si system [J]. Metallurgical and Materials Transactions A, 1995, 26(2): 243−257.

[20] RAMACHANDRA C, SINGH V. Silicide precipitation in alloy Ti−6Al−5Zr−0.5Mo−0.25Si [J]. Metallurgical Transactions A, 1982, 13(5): 771−775.

[21] POPOV A, ZHILYAKOVA M A, ELKINA O, LUGOVAYA K I. The precipitation of silicide particles in heat-resistant titanium alloys [C]//Advanced Methods and Technologies in Metallurgy in Russia: Springer, Cham, 2018: 19−25.

[22] JIA Weri-ju, ZENG Wei-dong, YU Han-qing. Effect of aging on the tensile properties and microstructures of a near-alpha titanium alloy [J]. Materials & Design, 2014, 58: 108−115.

[23] RAMACHANDRA C, SINGH V. Silicide phases in some complex titanium alloys [J]. Metallurgical Transactions A, 1992, 23(2): 689−690.

[24] RAMACHANDRA C, SINGH V. Orientation relationship between α' titanium and silicide S_{02} in alloy Ti−6Al−5Zr−0.5Mo−0.25 Si [J]. Metallurgical Transactions A, 1985, 16(3): 453−455.

[25] RAMACHANDRA C, SINGH V. Silicide precipitation in alloy Ti−6Al−5Zr−0.5Mo−0.25Si [J]. Metallurgical Transactions A, 1982, 13(5): 771−775.

[26] BANERJEE D. On the structural determination of silicides in titanium alloys [J]. Scripta Metallurgica, 1987, 21(12): 1615−1617.

[27] HONG Quan, QI Yun-lian, GUO Ping, ZENG Li-ying, ZHAO Yong-qing. Study on the microstruction characteristic and creep properties of Ti600 alloy [J]. Materials China, 2007, 26(9): 19−22.

[28] RAMOS A S, NUNES C A, COELHO G C. On the peritectoid Ti_3Si formation in Ti−Si alloys [J]. Materials Characterization, 2006, 56(2): 107−111.

[29] GU Yi, ZENG Fan-hao, QI Yan-ling, XIONG Xiang. Tensile creep behavior of heat-treated TC11 titanium alloy at 450−550 ℃ [J]. Materials Science and Engineering A, 2013, 575: 74−85.

[30] LIU Cui-ping. Twinning deformation and plasticity and toughness of α titanium alloys [D]. Shaanxi, China: Xi'an University of Technology, 2005.

[31] CHRISTIAN J W, MAHAJAN S. Deformation twinning [J]. Progress in Materials Science, 1995, 39(1/2): 1−157.

[32] SUN J L, TRIMBY P W, YAN F K, LIAO X Z, TAO N R, WANG J T. Grain size effect on deformation twinning propensity in ultrafine-grained hexagonal close-packed titanium [J]. Scripta Materialia, 2013, 69(5): 428−431.

[33] CHOI S H, KIM J K, KIM B J, KIM B J, PARK Y B. The effect of grain size distribution on the shape of flow stress curves of Mg−3Al−1Zn under uniaxial compression [J]. Materials Science and Engineering A, 2008, 488: 458−467.

[34] STAPLETON A M, RAGHUNATHAN S L, BANTOUNAS I, STONE H J, LINDLEY T C, DYE D. Evolution of lattice strain in Ti−6Al−4V during tensile loading at room temperature [J]. Acta Materialia, 2008, 56: 6186−6196.

[35] MEYERS M A. VÖHRINGER O, LUBARDA V A, The onset of twinning in metals: A constitutive description [J]. Acta Materialia, 2001, 49: 4025−4039.

[36] MAHAJAN S, WILLIAMS D F. Deformation twinning in metals and alloys [J]. International Metallurgical Reviews, 1973, 18(2): 43−61.

[37] FITZNER A, PRAKASH D G L, FONSECA J Q D, THOMAS M, ZHANG Shu-yan, KELLEHER J, MANUEL P, PREUSS M. The effect of aluminium on twinning in binary alpha-titanium [J]. Acta Materialia, 2016, 103: 341−351.

[38] LAI Xin-min, PENG Lin-fa, HU Peng, LAN Shu-huai, NI Jun. Material behavior modelling in micro/meso-scale forming process with considering size/scale effects [J]. Computational Materials Science, 2008, 43(4): 1003−1009.

[39] CHAN W L, FU M W. Studies of the interactive effect of specimen and grain sizes on the plastic deformation behavior in microforming [J]. The International Journal of Advanced Manufacturing Technology, 2012, 62(9): 989−1000.

[40] LIN Xiao-juan. Study of numerical simulation modeling of micro thickness sheet metal forming and size effect of bending springback [D]. Jinan, China: Shandong University, 2014.

[41] MA Zhen-wu. Research on size effects of TC1 foils bend forming and their applications [D]. Jiangsu, China: Nanjing University of Aeronautics and Astronautics, 2017.

[42] FU M W, CHAN W L. Micro-scaled products development via microforming [M]//Springer series in advanced manufacturing. London: Springer, 2014.

$\alpha+\beta$ 固溶处理对 Ti65 合金薄板的影响：硅化物析出、力学行为和新型$\{10\bar{1}1\}$孪晶系

赵 鼎[1]，樊江昆[1,2,3]，张智鑫[1,4]，王 璟[1]，王清江[5]，陈志勇[5]，唐 斌[1,2]，寇宏超[1,2]，李金山[1,2]

1. 西北工业大学 凝固技术国家重点实验室，西安 710072；
2. 西北工业大学 重庆科创中心，重庆 401135；
3. 西北工业大学 先进金属材料精确热成型技术国家地方联合工程研究中心，西安 710072；
4. 宝钛集团有限公司，宝鸡 721014；
5. 中国科学院 金属研究所，沈阳 110016

摘 要：为应对航空领域对轻质和优异高温性能钛合金部件的迫切需求，对经不同热处理的新型高温钛合金 Ti65 合金薄板的显微组织演变、硅化物析出和力学行为进行系统研究。结果表明：在固溶空冷后的合金中析出亚微米级硅化物$(Ti,Zr)_6Si_3$，导致拉伸性能变差和剧烈波动。在 950 ℃固溶炉冷后的合金中发现穿晶界$(Ti,Zr)_5Si_3$和近晶界$(Ti,Zr)_6Si_3$硅化物的共存。当固溶温度升高至 1010 ℃时，$(Ti,Zr)_3Si$硅化物在位错附件出现。薄板固有尺寸效应与硅化物析出的协同效应导致拉伸性能的明显波动，塑性显著下降，甚至发生脆性断裂。硅化物析出受低温固溶处理的保温时间的影响较弱。此外，在 990 ℃热轧获得的薄板中观察到新型$\{10\bar{1}1\}$孪晶，其轴角对为 $65°\langle 8\bar{4}\bar{4}3\rangle$，仅存在于粗大的基面织构 α 晶粒中。

关键词：钛合金；薄板；硅化物；力学性能；尺寸效应；孪晶

(Edited by Bing YANG)